21st Annual Conference of the Canadian Nuclear Society
Toronto, Ontario, Canada / June 11-14, 2000

The Analytic Nodal Method for CANDU Reactor Three-Dimensional Space-Time Kinetics Calculations

Jinchao Mao and Jean Koclas

Institut de Génie Nucléaire

École Polytechnique de Montréal

C.P. 6079, Succ. Centre-ville Montréal (Québec), Canada H3C 3A7

Abstract

The Analytic Nodal Method (ANM) is noted as an accurate and efficient numerical method for solving the multidimensional, two-group kinetics neutron-diffusion equation. The only approximation introduced during the derivation of ANM is the shape of the transverse leakage. The spatial coupling is determined by the analytic solution of one-dimensional diffusion equations. The resulting super-matrix equations can be written in terms of node-averaged fluxes and face-averaged net leakages, and have the form of a classical eigenvalue problem which can be solved by the standard source iteration procedure. The Analytic Nodal Method has been implemented in the code NDF, and tested for two CANDU problems. The calculations clearly indicate that the ANM is more accurate than the Coarse Mesh Finite Difference (CMFD) method for CANDU analysis.

1. Introduction

Nodal methods have been used for Light Water Reactors (LWR) core-physics and safety analysis for more than 20 years. In the past two decades, the modern nodal methods, for example, the Nodal Expansion Method (NEM) (Finnemann et al., 1977), the Analytic Nodal Method (ANM) (Smith, 1979), and the Nodal Green's Function method (NGFM) (Lawrence et al., 1980), have successfully been developed to solve the spatial problem of the LWR. However, in the case of heavy-water systems, primarily because of the large neutron migration area, the Coarse Mesh Finite Difference Method (CMFD) has been found to be adequate and has been extensively

used for CANDU analysis in the past 30 years. To address the increased accuracy requirements of current and future analysis, the use of nodal method as an alternative tool for CANDU analysis is being investigated.

Among numerous advanced nodal methods, ANM is noted as an accurate and efficient numerical method for solving the multidimensional, 2-group kinetics neutron-diffusion equations for LWR. The ANM-based QUANDRY code (Smith, 1979) cannot be used directly for CANDU analysis because it was specifically designed for LWR. A large number of difficulties would be encountered for QUANDRY to perform 3-D CANDU transient analysis with the reactivity devices inserted and moving perpendicular to the fuel. An alternate way is to review the ANM formalism and develop independent modules into a current CANDU diffusion code, such as the NDF code (Kaveh et al., 1999) used in this study. As a bonus, such an implementation of the ANM permits using the latest DRAGON generated cross-section sets, and access to DONJON utilities for handling reactivity devices.

The objectives of the paper are divided into two parts. First we very briefly review the derivation procedure of Analytic Nodal Method with a flat transverse leakage approximation, which is the only approximation introduced during the derivation. A suitable iterative scheme employed for solving the static and kinetic equations will also be described. The second objective is to apply the Analytic Nodal Method to the CANDU benchmark problem and a typical CANDU-6 problem, both for static and dynamic cases. The solution from Analytic Nodal Method is compared with the solution from CMFD method.

2. Descriptions of the Methods

2.1 Coarse Mesh Finite Difference Method

MANY METHODS FOR SOLVING THE MULTIGROUP KINETIC DIFFUSIONS ARE PRESENTLY AVAILable to the nuclear reactor community. The most extensively and widely used method for CANDU reactor is the Coarse Mesh Finite Difference Method. This method is conceptually simple and the resulting algebraic equations are such that only adjacent nodes are coupled by the flux terms, which result in simple sparse matrix structures. One very important property of this finite difference method is that it can be shown to converge to the exact solution of the multigroup diffusion equations in the limit of infinitely fine mesh spacing. Also, as a consequence of the wide-use of

this and other similar methods, the associated numerical techniques have reached high levels of sophistication. The main disadvantage of CMFD is that a large number of mesh points are required to achieve acceptable accuracy in regions where the neutron flux is rapidly changing.

Recent research (Koclas, 1998) has shown that the CMFD could be obtained from the Analytic Nodal Method by setting to zero the transverse leakage terms, and by truncating the expansion of the matrix exponentials to first order terms. This indicates that the CMFD is the lowest order of all nodal methods. Therefore, using a true nodal method is expected to generate more accurate results for CANDU reactor analysis.

2.2 Analytic Nodal Method

ANOTHER CLASS OF TECHNIQUES USED TO SOLVE THE MULTIGROUP DIFFUSION EQUATIONS IS the nodal methods. During the past 20 years, the nodal methods have been used successfully for Light Water Reactors (LWR) and Boiling Water Reactors (BWR) core-physics and safety analysis. But they are seldom used for the CANDU reactor because the CMFD has generally been found to be adequate, even with the equivalent of one mesh point per fuel bundle.

The quantities of interest in most nodal methods are the group-dependent neutron fluxes averaged over large spatial regions (nodes) and the neutron currents averaged over the faces of the nodes. No approximations to the formally exact neutron transport equation need to be made in the derivation of the nodal balance equation. The difficulty with any nodal method is that the relationships between the node-averaged fluxes and the face-averaged currents must be known. Once these relationships are specified, the nodal equations can be constructed. Many different schemes have been proposed to determine the flux-current coupling. Compared with other nodal methods, the Analytic Nodal Method uses only one approximation for the coupling terms, this approximation being the transverse-leakage “shape”.

The flat transverse leakage approximation and the quadratic transverse leakage approximation are the two commonly used approximations. We use the flat transverse leakage approximation for this investigation, for the following reasons:

- In CANDU reactors, the net currents are very small when compared to the fluxes, which means that the transverse leakage s also will be small in value relative to the fluxes.
- For CANDU reactors, CMFD is generally acceptable, and it uses a zero transverse leakage approximation.

On this basis, it is reasonable to use the flat transverse leakage approximation in the analysis of the CANDU reactor.

The Analytic Nodal Method which employs analytic solutions of the one-dimensional, two-group diffusion equations to determine the spatial coupling coefficients. The final resulting super-matrix equations can be written in terms of nodal-averaged fluxes and face-averaged net leakages. The detailed derivation procedure will not be presented in this paper. It can be found in (Smith, 1979) and (Mao, 2000). Finally the three-dimensional, two-group kinetics diffusion equations used for ANM can be written as:

$$\begin{bmatrix} [V]^{-1} & [0] & [0] & [0] \\ [0] & [0] & [0] & [0] \\ [0] & [0] & [0] & [0] \\ [0] & [0] & [0] & [0] \end{bmatrix} \frac{\partial}{\partial t} \begin{bmatrix} [\bar{\phi}(t)] \\ [\bar{L}_x(t)] \\ [\bar{L}_y(t)] \\ [\bar{L}_z(t)] \end{bmatrix} = \left[\mathcal{F}\mathcal{G}\right] \begin{bmatrix} [\bar{\phi}(t)] \\ [\bar{L}_x(t)] \\ [\bar{L}_y(t)] \\ [\bar{L}_z(t)] \end{bmatrix} + \sum_{d=1}^{D} \begin{bmatrix} V_{i,j,k}[\chi^d]\lambda_d \bar{C}_{d,i,j,k}(t) \\ [0] \\ [0] \\ [0] \end{bmatrix} \quad \text{(EQ 1)}$$

and

$$\frac{\partial}{\partial t}[\bar{C}_d(t)] = [M_d(t)][\bar{\phi}(t)] - \lambda_d[\bar{C}_d(t)] \; d=1,2,3(\ldots, D) \quad \text{(EQ 2)}$$

where $[\bar{L}_z(t)]$, $[\bar{L}_y(t)]$ and $[\bar{L}_z(t)]$ represent the transverse leakage terms of the nodes of the reactor model. The leakage terms are simply the differences between the face average net currents of the corresponding surfaces of the nodes for each direction. The details of the matrix $\left[\mathcal{F}\mathcal{G}\right]$ are quite involved and can be found in (Smith, 1979) or (Mao, 2000).

3. Numerical Techniques

3.1 Static Neutron-Diffusion Calculation

If we set the temporal derivatives of equation (1) to zero, the static equation for which a solution is sought in the Analytic Nodal Method can be obtained. It is given by the following equation,

$$[H][\psi] = \frac{1}{\gamma}[P][\psi] \quad \text{(EQ 3)}$$

where

$$[\psi] \equiv \mathrm{col}\left\{\left[[\phi]\ [\bar{L}_x]\ [\bar{L}_y]\ [\bar{L}_z]\right]\right\}$$

The super-matrix equation is a set of linear equations in the four vector unknowns: node-averaged flux, face-averaged net leakage for each direction. The equation has the form of a classical generalized eigenvalue problem, except for the fact that the coefficient matrix are eigenvalue dependent. In order to avoid some undesirable characteristics, the last three blocks of leakage equations are substituted into the first block of the flux equation. The general iterative scheme for solving this equation is as following:

1. An initial guess for γ (usually $\gamma = 1.5$) is used to evaluate the components of the coefficient matrix.
2. An accelerated fission source (outer) iteration is employed to determine iteratively the maximum eigenvalue and corresponding eigenvector.
3. After several outer iterations (usually 5 to 10), the latest estimate of γ is used to update the components of the coefficient matrix.
4. Use "modified" block Gauss-Seidel iteration method to perform the inner iteration.
5. Cyclic Chebyshev Semi(CCSI) iteration method or Gauss-Seidel iteration method is used for flux iteration.

The fact that the coefficient matrix depends on the eigenvalue of the global static reactor problem gives the outer iterations a nonlinear character. The general practice of updating the matrices every 5 to 10 outer iterations (Smith, 1979) seems entirely appropriate. The eigenvalue shift technique employed during the outer iterations significantly increases the convergence rate of the outer iterations.

The inner iteration consists of two steps. First, the new node-averaged fluxes are determined from the old fission source and the old leakages. Secondly, the new net leakages are determined by the new fluxes and old leakages.

Normally only one inner iteration per outer iteration is considered sufficient because the leakages are so small compared to the flux. The node-flux iteration can be done by Cyclic Chebyshev Semi-Iteration (CCSI) method or Gauss-Seidel iteration method. The iteration keeps on until convergence reached.

3.2 Kinetics Neutron-Diffusion Calculation

The kinetics equations of ANM are shown by equations (1) and (2). Only the first block of equation (1) involves a temporal operator. The latter three blocks are simply expressions for the transverse leakages at time t and do not involve temporal operators. Hence any time integration scheme which approximates the temporal derivatives can be employed to solve the kinetic equations. We used the fully implicit method as the time iteration method in this work. A description of kinetics solution algorithm is outlined below:

1. Choose the times $(0, T_1, T_2, T_3 \ldots T_i)$ which divide the kinetics problem into time domains within each time step.
2. Assume the initial values of $[\bar{\phi}]^n$, $[\bar{L}_u]^n$ and $[\bar{C}_d]^n$ are known at time t_n.
3. If $t_n = T_i$, change Δt and the flux convergence criterion ϵ to correspond to those of time domain i+1. Calculate new CCSI optimization parameters.
4. Alter cross sections to correspond to core status at time t_{n+1}.
5. Calculate matrix elements.
6. Obtain approximations for $[\bar{\phi}]^{n+1}$ and $[\bar{L}_u]^n$ by extrapolation procedure.
7. Perform flux iteration to get $[\bar{\phi}]^{n+1}$ and $[\bar{L}_u]^{n+1}$.
8. Solve the equations for $[\bar{C}_d]^{n+1}$.
9. Calculate new extrapolation frequencies for the next time step.
10. Repeat steps 3-9 for each time step until the end of the last time domain.

The complete matrices updating can be performed every 3 to 10 time steps. The CCSI or successive over-relaxation (SOR) flux iterations can be used. As the leakages and fluxes are estimated by an extrapolation procedure, the computational effort required to solve the kinetics nodal diffusion equations is significantly reduced.

Based on the above formulation and iteration scheme, the modules with the Analytic Nodal Method for solving both the 3-D static and kinetics neutron diffusion equations have been developed and fully implemented in the code NDF. Two CANDU problems were tested for the Analytic Nodal Method. Both static and kinetics results will be presented separately in the following two sections, as well as the comparison with the fine-mesh and coarse-mesh CMFD results.

4. Static Results

4.1 The 3-D CANDU Benchmark Problem

The 3-D CANDU benchmark problem (ANL, 1985) is a simplified three-dimensional, two-group kinetics benchmark problem as described in Appendix A. It has been proven as a very important standard by which progress in CANDU calculation methods have been measured. We use the results from a fine-mesh (72 x 72 x 40) CMFD calculation as the reference.

Table 1 summarizes the main calculation results of this problem. Figure 1 exhibits the nodal power density distributions and percent errors of ANM (18 x 18 x 10) and CMFD (18 x 18 x 10). It is found that the maximum error of nodal power densities for ANM and CMFD are about 4.3% and 5.9% respectively; these are located in the node (14,5,5) for CMFD, and (5,5,2) for ANM. These results show that the nodes with larger percent errors of power densities are in lower power regions, near the reflector. A detailed comparison of solutions from CMFD method and ANM method illustrates that with the same mesh size, the ANM consistently gets the more accurate solution, as expected.

The graphs of normalized nodal power density distributions on plane 5, of absolute percent errors in nodal power densities on plane 5, and of transverse leakages of the thermal group on plane 5 are given in Figures 2, 3 and 4.

4.2 The Typical CANDU-6 problem

The typical CANDU-6 problem (Koclas, 1998, and Arias, 1996) is a simplified 3-D full core, 2-energy-group model of CANDU reactor, with main reactivity devices, such as liquid zone controllers and adjuster rods are present in the core. This problem is much like a true CANDU-6 reactor core, in contrast to the CANDU benchmark problem. This model is introduced for the purpose of full-core dynamic simulations. The problem is somewhat simplified, as the axial notch in the reflector is not present in this model, and many small in-core structures are not represented.

The fuel and reactivity device macroscopic cross-sections were calculated by the DRAGON/DONJON chain code (Marleau et al., 1993,1994; Roy et al., 1993). The detailed description of this problem is in Appendix B. We use the results from a fine mesh (104 x 104 x 48) CMFD calculation as the reference.

Table 2 summarizes the main calculation result of this problem. Figures 5 and 6 exhibit the channel power density distributions and percent errors of ANM (26 x 26 x 12) and CMFD (26 x 26 x 12).

The results indicate that CMFD and ANM-derived eigenvalues, maximum channel power and maximum bundle power agree well with the reference values. Compared with the reference values, the average and maximum errors in ANM-predicted channel and bundle power densities are all smaller than those predicted with CMFD. The maximum error of bundle power densities for ANM and CMFD are about 2.8% and 6.0% respectively; the maximum error of channel power densities for ANM and CMFD are about 1.6% and 2.2% respectively. For ANM calculations, the maximum percent errors of channel and bundle power densities are located at W13 and (W14, 4) respectively, which is in the core periphery region adjacent to the reflector. Overall, comparison between CMFD and ANM shows that the ANM results are more accurate as expected.

The Xenon effect of this problem also has been calculated by CMFD and ANM respectively. The results of Xenon effect are summarized in Table 3. Figure 7 illustrates the Xenon effect on the channel power density distributions. The results indicate the difference of Xenon reactivity between CMFD and ANM is only about 0.038mk. The power distributions tend to be flatter on account of the Xenon effect.

5. Kinetics results

5.1 The CANDU Benchmark Problem

A simplified three-dimensional CANDU benchmark problem (ANL, 1985), with asymmetric effects due to both a LOCA and shut-off rods insertion, is used for the purpose of checking our implementation of the ANM in the NDF code. A detailed description of the benchmark can be found in Appendix A.

In order to evaluate the accuracy of the different methods, it is necessary to have a reference solution. Unfortunately, all the published solutions for this problem were from Coarse Mesh Finite Difference Method with a very coarse spatial mesh (18 x 18 x 10), which is not considered suitable as the reference. Hence a Coarse Mesh Finite Difference Method results with (54 x 54 x 30) spatial meshes from NDF calculation is used as the reference in this study. The reference calculations use a time step size of 12.5 ms. These calculations employed a flux convergence criterion of 10^{-6}.

Figures 8 to 14 show the results from ANM and CMFD. Comparison of the percent errors of total power obtained by ANM and CMFD with the same time step and same mesh size indicates that the time-dependent total power predicted by the Analytic Nodal Method has an excellent agreement with the reference values. The maximum error in total power is of 3%, and there is no significant

loss of accuracy for Analytic Nodal Method during the transient. The difference between the Coarse Mesh Finite Difference Method results and the reference values is small (slightly larger than the ANM results) in the beginning of the transient and increases quickly in the first 1.2 seconds and reaches about 13% after 1.8 seconds, which is not considered negligible. Similar conclusions are observed for the transient nodal power predictions. This significant decrease in accuracy indicates that the CMFD is not as reliable as the ANM for rapid transient scenarios with significant leakage distribution in the core. To improve the calculation accuracy, either the CMFD with a fine-mesh (such as the 54x54x 30 used as reference) or a nodal method, such as ANM, should be applied.

5.2 The Typical CANDU-6 Problem

In this case, we perform a rod-ejection simulation. The transient is initiated by instantaneous withdrawal of the first bank consisting of 5 adjuster rods, initially in the core, as shown in Figure A1.7. The resulting transient is followed for 900 seconds. The detailed description of this problem can be found in Appendix B.

The reactor regulation system is used in this problem, but Shutdown Systems were disabled. All the devices are initially set to nominal positions:14 LZC to 50%, 21 adjusters fully inserted (Marleau et al., 1996; Varin et al. 1996). Each device is then moved and set to a new position independently based on the results of the reactor regulating system algorithms. No reference solution is available for this problem. Hence it is difficult to measure, in absolute sense, the errors in the solution of the Analytic Nodal Method and Coarse Mesh Finite Difference Method.

The Analytic Nodal Method calculations employed the mesh size (26 x 26 x 12) and the time step size of 25 ms. The convergence criterion was 10^{-6}. The Coarse Mesh Finite Difference Method calculations used the same mesh size, same time step, and same convergence criterion.Figures 15, 16, 17 shows the results of ANM. All the results exhibit that the curve obtained from Analytic Nodal Method is similar to the curve obtained from Coarse Mesh Finite Difference Method. This serves as a supplementary demonstration that the Analytic Nodal Method is a viable, powerful alternative method for the simulation of CANDU reactors.

6. Conclusions

Calculation results with the Coarse Mesh Finite Difference Method show that it is generally adequate for static CANDU analysis, and the difference between CMFD and ANM is found to be not very important. However for transient scenarios, with significant leakages or flux

tilts, the difference between CMFD and ANM can not be considered as negligible. With the increased accuracy requirements of current and future analysis, either a finer mesh with finite differences or a standard mesh with higher order nodal methods will have to be applied for CANDU analysis.

Results from a CANDU benchmark and and typical CANDU-6 model demonstrate that accurate kinetics solutions could be obtained with the Analytic Nodal Method by using bundle size spatial meshes. Comparisons with Coarse Mesh Finite Difference Method indicated that the errors produced by the Analytic Nodal Method were consistently lower.

The Analytic Nodal Method with flat leakage approximation is thus shown to be a superior method to CMFD for solving the multidimensional two-group static or kinetics diffusion equation in the context of the CANDU reactor.

7. Acknowledgments

Part of this work was supported by a grant from the Natural Science and Engineering Research Council of Canada.

Table 1: Summary of the static results for the 3-D CANDU benchmark problem

	Coarse Finite Difference Method (CMFD)	Analytic Nodal Method (ANM)
Outer iterations	32	132
Eigenvalue	1.00355	1.00318
$\varepsilon_{\max}(I,J,K)(nodal\ ,\%)$	5.889 (14,5,5)	4.253 (5,5,2)
$\bar{\varepsilon}\ (nodal\ ,\%)$	1.419	0.847
$P_{\max}(I,J,K)\ \ (nodal\ )$	1.934 (10,13,5),(9,13,5)	1.914 (10,13,5),(13,10,5)
Execution time (s)	1.32	12.26

Reference eigenvalue: 1.00338
Reference maximum nodal power density: 1.897
Outer iteration convergence criterion: 10^{-6}
Flux iteration convergence criterion: 10^{-6}

Table 2: Summary of the static results for the 3-D typical CANDU-6 without Xenon effect problem

	Coarse Finite Difference Method (CMFD)	Analytic Nodal Method (ANM)
Outer iterations	91	93
Eigenvalue	1.03067	1.03047
$\varepsilon_{\max}(I,J)(channel,\%)$	2.176 (G21)	1.606 (W11)
$\bar{\varepsilon}\ (channel,\%)$	0.735	0.516
$P_{\max}(I,J)\ \ (channel\ )$	1.249 (E14)	1.246 (F15)
$\varepsilon_{\max}(I,J,K)(bundle\ ,\%)$	6.045 (K12,8)	2.792 (W12,4)
$\bar{\varepsilon}\ (bundle\ ,\%)$	1.552	0.646
$P_{\max}(I,J,K)\ \ (bundle\ )$	1.853 (E12,6)	1.843 (E12,6)
Execution time (s)	13.74	42.85

Reference eigenvalue: 1.03057
Reference maximum channel power density: 1.250
Reference maximum bundle power density: 1.846
Outer iteration convergence criterion: 10^{-6}
Flux iteration convergence criterion: 10^{-5}

Table 3: Summary of results for the 3-D typical CANDU-6 with Xenon effect problem

	Coarse Finite Difference Method (CMFD)	Analytic Nodal Method (ANM)
Eigenvalue	1.00275	1.00258
Xenon Reactivity (mk)	-26.952	-26.990
$P_{\max}(I,J,K)\ \ (bundle\ )$	1.845 (E11,6)	1.835 (E12,6)

Total reactor power is 2.154 x 10^9 w

	3	4	5	6	7	8	9	10	11	12	13	14	15	16
3					0.99	1.25	1.37	1.37	1.25	0.99				
					-1.97	-1.65	-1.83	-1.83	-1.65	-1.97				
					-2.83	-1.52	-1.29	-1.29	-1.52	-2.83				
4					1.27	1.53	1.66	1.66	1.53	1.27				
					0.59	1.53	1.48	1.48	1.53	0.59				
					-1.56	0.22	0.45	0.45	0.22	-1.56				
5			1.02	1.25	1.50	1.75	1.86	1.86	1.75	1.50	1.25	1.02		
			-5.89	-2.87	1.42	1.76	1.78	1.78	1.76	1.42	-2.87	-5.89		
			-4.25	-3.36	-0.60	0.58	0.83	0.83	0.58	-0.59	-3.36	-4.25		
6			1.25	1.42	1.63	1.81	1.90	1.90	1.81	1.63	1.42	1.25		
			-2.87	0.06	1.58	1.89	1.97	1.97	1.89	1.58	0.06	-2.87		
			-3.36	-1.33	-0.10	0.65	0.89	0.90	0.66	-0.10	-1.33	-3.36		
7	0.99	1.27	1.50	1.63	1.60	1.64	1.66	1.66	1.64	1.60	1.63	1.50	1.27	0.99
	-1.97	0.59	1.42	1.58	-1.10	-1.11	-1.12	-1.12	-1.11	-1.10	1.58	1.42	0.59	-1.97
	-2.83	-1.56	-0.59	-0.10	0.26	0.55	0.78	0.78	0.56	0.26	-0.09	-0.59	-1.56	-2.83
8	1.25	1.53	1.75	1.81	1.64	1.54	1.51	1.51	1.54	1.64	1.81	1.75	1.53	1.25
	-1.65	1.54	1.76	1.89	-1.11	-0.90	-0.84	-0.84	-0.90	-1.11	1.89	1.76	1.54	-1.65
	-1.52	0.22	0.59	0.66	0.55	0.31	0.32	0.32	0.32	0.56	0.66	0.59	0.23	-1.51
9	1.37	1.66	1.86	1.90	1.66	1.51	1.45	1.45	1.51	1.66	1.90	1.86	1.66	1.37
	-1.83	1.49	1.78	1.97	-1.11	-0.84	-0.71	-0.71	-0.84	-1.11	1.97	1.78	1.49	-1.83
	-1.29	0.46	0.83	0.90	0.78	0.32	0.14	0.14	0.33	0.78	0.90	0.84	0.46	-1.28
10	1.37	1.66	1.86	1.90	1.66	1.51	1.45	1.45	1.51	1.66	**1.90**	1.86	1.66	1.37
	-1.83	1.49	1.78	1.97	-1.11	-0.84	-0.71	-0.71	-0.84	-1.11	1.97	1.78	1.49	-1.83
	-1.29	0.46	0.83	0.90	0.78	0.32	0.14	0.14	0.33	0.78	0.90	0.84	0.46	-1.28
11	1.25	1.53	1.75	1.81	1.64	1.54	1.51	1.51	1.54	1.64	1.81	1.75	1.53	1.25
	-1.65	1.54	1.76	1.89	-1.11	-0.90	-0.84	-0.84	-0.90	-1.11	1.89	1.76	1.54	-1.65
	-1.51	0.22	0.59	0.66	0.56	0.31	0.33	0.33	0.32	0.56	0.66	0.59	0.23	-1.51
12	0.99	1.27	1.50	1.63	1.60	1.64	1.66	1.66	1.64	1.60	1.63	1.50	1.27	0.99
	-1.97	0.59	1.42	1.58	-1.10	-1.11	-1.12	-1.12	-1.11	-1.10	1.58	1.42	0.59	-1.97
	-2.83	-1.56	-0.59	-0.09	0.26	0.56	0.78	0.78	0.56	0.27	-0.09	-0.59	-1.55	-2.82
13			1.25	1.42	1.63	1.81	1.90	1.90	1.81	1.63	1.42	1.25		
			-2.87	0.06	1.58	1.89	1.97	1.97	1.89	1.58	0.06	-2.87		
			-3.36	-1.33	-0.09	0.66	0.90	0.90	0.66	-0.09	-1.32	-3.35		
14			1.02	1.25	1.50	1.75	1.86	1.86	1.75	1.50	1.25	1.02		
			-5.89	-2.87	1.42	1.76	1.78	1.78	1.76	1.42	-2.87	-5.89		
			-4.25	-3.36	-0.59	0.59	0.83	0.83	0.59	-0.59	-3.35	-4.24		
15					1.27	1.53	1.66	1.66	1.53	1.27				
					0.59	1.53	1.48	1.48	1.53	0.59				
					-1.56	0.22	0.46	0.46	0.23	-1.55				
16					0.99	1.25	1.37	1.37	1.25	0.99—*Reference nodal power densities*				
					-1.97	-1.65	-1.83	-1.83	-1.65	-1.97--*Percent errors for CMFD (18 x18 x10)*				
					-2.83	-1.51	-1.28	-1.28	-1.51	-2.83--*Percent errors for ANM (18 x 18 x10)*				

Reference is the result of CMFD (72 x 72 x 40)
The maximum percent errors are shown in bold character

Figure 1: Comparison of percent errors in nodal power densities from CMFD (18 x 18 x 10) and ANM (18 x 18 x 10) for of the CANDU benchmark problem (plane 5)

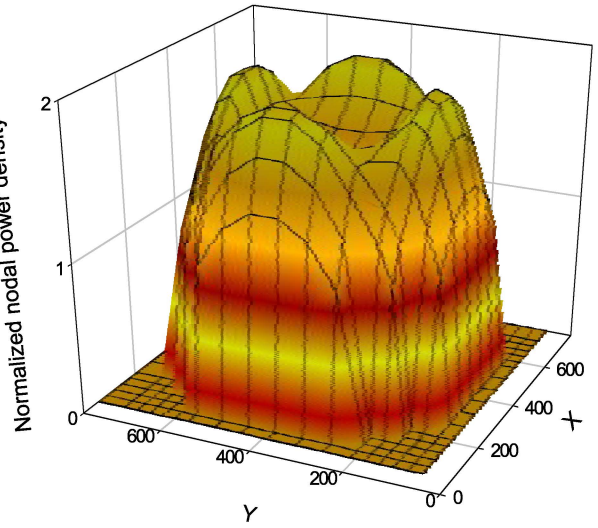

Figure 2: Normalized nodal power density distributions on plane 5 of the CANDU benchmark problem for ANM (18 x 18 x 10)

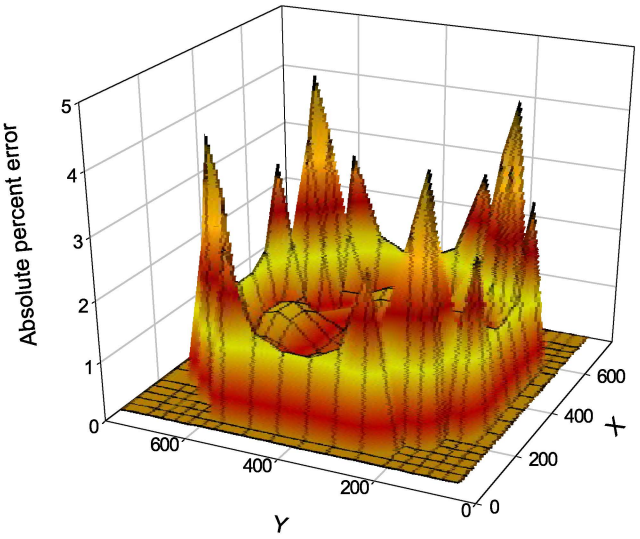

Figure 3: Absolute percent errors of nodal power densities on plane 5 of the CANDU benchmark problem for ANM (18 x 18 x10)

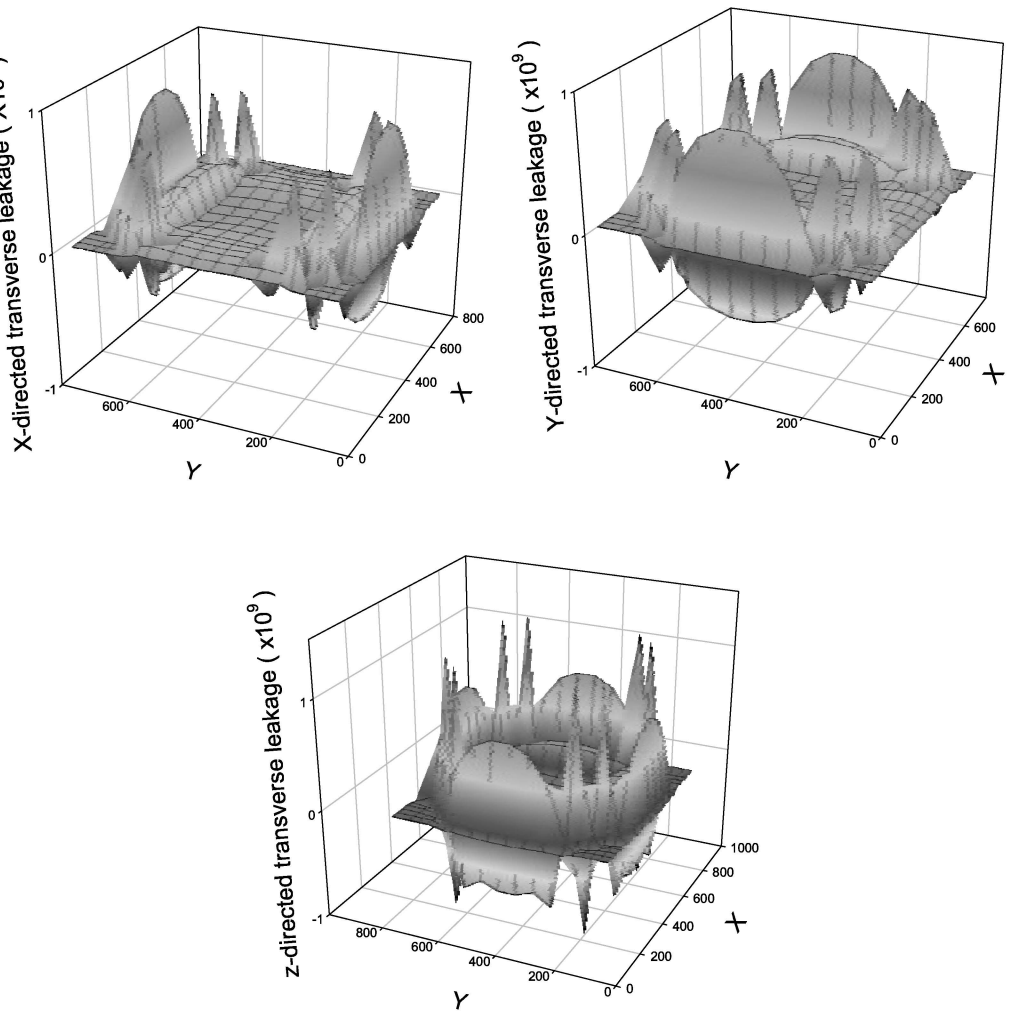

Figure 4: Transverse leakages of thermal group on plane 5 of the CANDU benchmark problem for ANM (18 x 18 x10)

	1	2	3	4	5	6	7	8	9	10	11	12	13	14	15	16	17	18	19	20	21	22
A									0.57	0.62	0.64	0.64	0.62	0.57								
									0.12	1.01	1.25	1.22	0.93	-0.01								
B						0.51	0.63	0.73	0.80	0.85	0.87	0.87	0.85	0.81	0.73	0.63	0.51					
						-0.30	0.06	-0.17	0.56	0.73	0.99	0.96	0.65	0.42	-0.36	-0.18	-0.59					
C					0.57	0.71	0.85	0.95	1.02	1.05	1.05	1.05	1.05	1.02	0.95	0.85	0.72	0.58				
					-0.34	0.86	0.72	0.65	0.55	0.45	0.83	0.80	0.36	0.40	0.44	0.47	0.56	-0.68				
D				0.59	0.75	0.90	1.03	1.12	1.17	1.18	1.16	1.16	1.18	1.17	1.12	1.04	0.91	0.75	0.59			
				-0.63	0.83	0.84	0.59	0.52	0.41	0.19	0.66	0.62	0.09	0.25	0.30	0.32	0.52	0.47	-1.02			
E			0.56	0.74	0.91	1.05	1.16	1.22	1.24	1.24	1.21	1.21	1.24	1.24	1.22	1.16	1.06	0.92	0.75	0.56		
			-0.69	0.51	0.80	0.65	0.43	0.27	0.20	-0.10	0.25	0.21	-0.21	0.03	0.04	0.15	0.32	0.42	0.10	-1.12		
F			0.69	0.88	1.03	1.14	1.21	1.24	1.22	1.20	1.18	1.18	1.20	1.22	**1.25**	1.22	1.15	1.04	0.89	0.70		
			-0.43	0.46	0.63	0.41	0.28	-0.03	0.04	-0.25	-0.09	-0.13	-0.36	-0.14	-0.27	-0.01	0.07	0.24	0.03	-0.89		
G		0.60	0.81	0.99	1.11	1.19	1.21	1.22	1.20	1.18	1.17	1.17	1.18	1.20	1.23	1.22	1.19	1.11	0.99	0.81	0.60	
		-0.96	0.26	0.31	0.60	0.32	0.02	-0.34	-0.22	-0.42	-0.48	-0.52	-0.54	-0.41	-0.59	-0.28	-0.04	0.20	-0.14	-0.22	-1.46	
H		0.70	0.91	1.06	1.14	1.19	1.20	1.20	1.18	1.16	1.16	1.16	1.16	1.18	1.21	1.21	1.20	1.15	1.07	0.91	0.71	
		-0.30	0.38	0.15	0.64	0.26	-0.25	-0.56	-0.47	-0.61	-0.75	-0.79	-0.73	-0.66	-0.82	-0.57	-0.12	0.22	-0.31	-0.11	-0.81	
J	0.56	0.78	0.99	1.12	1.16	1.17	1.18	1.17	1.15	1.14	1.13	1.13	1.14	1.16	1.18	1.18	1.18	1.17	1.13	0.99	0.79	0.57
	0.18	0.54	0.38	0.03	0.51	0.04	-0.41	-0.64	-0.70	-0.85	-0.99	-1.03	-0.97	-0.90	-0.90	-0.74	-0.35	0.07	-0.44	-0.11	0.02	-0.36
K	0.62	0.85	1.04	1.16	1.18	1.16	1.17	1.15	1.13	1.11	1.09	1.09	1.11	1.14	1.16	1.17	1.17	1.18	1.17	1.05	0.85	0.62
	1.06	0.79	0.43	-0.02	0.51	0.04	-0.49	-0.69	-0.85	-1.03	-0.97	-1.02	-1.16	-1.05	-0.96	-0.83	-0.35	0.06	-0.49	-0.07	0.26	0.51
L	0.65	0.88	1.07	1.18	1.20	1.18	1.17	1.15	1.12	1.09	1.06	1.06	1.10	1.13	1.15	1.17	1.19	1.21	1.19	1.08	0.88	0.65
	1.08	0.84	0.48	0.07	0.47	0.04	-0.41	-0.69	-0.91	-1.14	-0.85	-0.90	-1.26	-1.11	-0.96	-0.75	-0.36	0.03	-0.40	-0.02	0.31	0.52
M	0.65	0.88	1.07	1.19	1.21	1.19	1.17	1.15	1.12	1.09	1.06	1.06	1.09	1.12	1.15	1.18	1.20	1.22	1.20	1.08	0.88	0.65
	1.08	0.86	0.53	0.17	0.50	0.08	-0.30	-0.63	-0.88	-1.14	-0.91	-0.95	-1.27	-1.08	-0.90	-0.64	-0.32	0.06	-0.30	0.03	0.33	0.53
N	0.61	0.84	1.04	1.17	1.21	1.19	1.17	1.15	1.13	1.10	1.07	1.07	1.10	1.13	1.16	1.18	1.20	1.21	1.18	1.05	0.85	0.62
	1.08	0.83	0.54	0.25	0.54	0.10	-0.20	-0.54	-0.76	-0.98	-0.83	-0.87	-1.11	-0.96	-0.81	-0.54	-0.28	0.10	-0.21	0.05	0.31	0.54
O	0.56	0.78	0.98	1.12	1.18	1.19	1.18	1.16	1.14	1.12	1.11	1.11	1.12	1.14	1.17	1.18	1.20	1.19	1.13	0.99	0.78	0.56
	0.21	0.60	0.51	0.31	0.54	0.11	-0.12	-0.47	-0.56	-0.70	-0.71	-0.75	-0.82	-0.76	-0.73	-0.44	-0.26	0.12	-0.14	0.02	0.10	-0.31
P		0.69	0.89	1.05	1.12	1.17	1.18	1.18	1.15	1.14	1.13	1.14	1.14	1.16	1.18	1.19	1.18	1.13	1.05	0.90	0.70	
		-0.23	0.48	0.27	0.68	0.29	-0.12	-0.40	-0.29	-0.41	-0.53	-0.57	-0.53	-0.47	-0.65	-0.43	-0.07	0.27	-0.17	0.01	-0.72	
Q		0.58	0.78	0.95	1.04	1.12	1.17	1.18	1.17	1.15	1.15	1.15	1.16	1.17	1.19	1.17	1.13	1.05	0.95	0.79	0.59	
		-0.89	0.30	0.26	0.82	0.43	0.00	-0.21	-0.01	-0.18	-0.32	-0.36	-0.28	-0.18	-0.44	-0.29	0.09	0.43	-0.16	-0.15	-1.36	
R			0.66	0.83	0.95	1.06	1.15	1.20	1.18	1.17	1.16	1.16	1.17	1.18	1.20	1.16	1.07	0.95	0.83	0.66		
			-0.44	0.33	0.96	0.56	0.20	0.09	0.27	0.08	0.18	0.15	-0.02	0.11	-0.13	-0.07	0.24	0.60	-0.07	-0.87		
S			0.53	0.69	0.83	0.97	1.09	1.16	1.19	1.20	1.17	1.17	1.20	1.20	1.17	1.10	0.98	0.84	0.69	0.53		
			-0.74	0.37	1.10	0.76	0.40	0.42	0.46	0.25	0.68	0.65	0.16	0.31	0.22	0.15	0.47	0.76	0.00	-1.14		
T				0.55	0.70	0.85	0.98	1.07	1.12	1.14	1.12	1.12	1.14	1.13	1.07	0.98	0.85	0.70	0.55			
				-0.65	0.95	0.96	0.72	0.71	0.69	0.48	0.96	0.93	0.39	0.54	0.52	0.49	0.68	0.64	-1.00			
U					0.54	0.68	0.81	0.91	0.98	1.01	1.00	1.00	1.01	0.98	0.91	0.81	0.68	0.55				
					-0.29	0.99	0.97	0.89	0.85	0.74	1.24	1.21	0.66	0.72	0.72	0.75	0.73	-0.59				
V						0.49	0.60	0.70	0.77	0.82	0.83	0.83	0.82	0.77	0.70	0.60	0.49					
						-0.15	0.34	0.12	0.88	1.12	1.44	1.41	1.04	0.76	-0.05	0.13	-0.39					
W									0.55	0.60	0.62	0.62	0.60	0.55	----------*Reference channel power densities*							
									0.45	1.43	**1.61**	1.58	1.36	0.34	----------*Percent errors for ANM (26 x 26 x 12)*							

Reference is the result of CMFD (104 x 104 x 48)

The maximum normalized channel power density and the maximum percent error are shown in bold character

Figure 5: Normalized channel power densities and percent errors of the typical CANDU-6 without Xenon effect problem for ANM (26 x 26 x 12)

	1	2	3	4	5	6	7	8	9	10	11	12	13	14	15	16	17	18	19	20	21	22
A									-1.05	-0.77	-1.24	-1.28	-0.88	-1.22								
									0.12	1.01	1.25	1.22	0.93	-0.01								
B						-1.12	-0.55	-0.13	0.90	0.87	0.56	0.52	0.75	0.70	-0.39	-0.87	-1.51					
						-0.30	0.06	-0.17	0.56	0.73	0.99	0.96	0.65	0.42	-0.36	-0.18	-0.59					
C					-0.45	1.13	1.08	1.00	0.97	0.87	0.69	0.65	0.74	0.77	0.72	0.73	0.72	-0.91				
					-0.34	0.86	0.72	0.65	0.55	0.45	0.83	0.80	0.36	0.40	0.44	0.47	0.56	-0.68				
D				-0.38	1.27	1.18	1.02	0.93	0.84	0.76	0.46	0.42	0.62	0.62	0.63	0.65	0.75	0.78	-0.91			
				-0.63	0.83	0.84	0.59	0.52	0.41	0.19	0.66	0.62	0.09	0.25	0.30	0.32	0.52	0.47	-1.02			
E			-1.03	1.22	1.19	0.97	0.91	0.87	0.82	0.75	0.40	0.35	0.61	0.58	0.56	0.52	0.51	0.67	0.65	1.63		
			-0.69	0.51	0.80	0.65	0.43	0.27	0.20	-0.10	0.25	0.21	-0.21	0.03	0.04	0.15	0.32	0.42	0.10	-1.12		
F			-0.12	1.11	0.88	0.66	0.37	0.16	-0.62	-0.79	-1.08	-1.13	-0.95	-0.86	-0.17	-0.04	0.18	0.34	0.52	-0.75		
			-0.43	0.46	0.63	0.41	0.28	-0.03	0.04	-0.25	-0.09	-0.13	-0.36	-0.14	-0.27	-0.01	0.07	0.24	0.03	-0.89		
G		-1.51	0.83	0.98	0.74	0.48	-0.14	-0.29	-0.63	-0.68	-0.67	-0.72	-0.84	-0.89	-0.63	-0.56	-0.02	0.19	0.36	0.18	**-2.18**	
		-0.96	0.26	0.31	0.60	0.32	0.02	-0.34	-0.22	-0.42	-0.48	-0.52	-0.54	-0.41	-0.59	-0.28	-0.04	0.20	-0.14	-0.22	-1.46	
H		-0.19	0.90	0.78	0.46	0.17	-0.20	-0.29	-0.65	-0.75	-0.81	-0.87	-0.92	-0.92	-0.66	-0.64	-0.35	-0.12	0.15	0.23	-0.88	
		-0.30	0.38	0.15	0.64	0.26	-0.25	-0.56	-0.47	-0.61	-0.75	-0.79	-0.73	-0.66	-0.82	-0.57	-0.12	0.22	-0.31	-0.11	-0.81	
J	-1.17	0.76	0.82	0.69	0.39	-0.33	-0.63	-0.70	-0.82	-0.88	-1.01	-1.07	-1.05	-1.10	-1.07	-1.08	-0.86	-0.21	0.04	0.14	0.05	-1.90
	0.18	0.54	0.38	0.03	0.51	0.04	-0.41	-0.64	-0.70	-0.85	-0.99	-1.03	-0.97	-0.90	-0.90	-0.74	-0.35	0.07	-0.44	-0.11	0.02	-0.36
K	-0.87	0.74	0.69	0.52	-0.07	-0.76	-0.68	-0.69	-0.86	-0.95	-1.15	-1.21	-1.12	-1.15	-1.07	-1.14	-1.29	-0.68	-0.14	-0.01	0.01	-1.61
	1.06	0.79	0.43	-0.02	0.51	0.04	-0.49	-0.69	-0.85	-1.03	-0.97	-1.02	-1.16	-1.05	-0.96	-0.83	-0.35	0.06	-0.49	-0.07	0.26	0.51
L	-1.18	0.63	0.70	0.68	0.47	-0.18	-0.49	-0.61	-0.84	-0.94	-1.21	-1.27	-1.12	-1.12	-0.99	-0.95	-0.72	-0.14	0.02	0.00	-0.09	-1.92
	1.08	0.84	0.48	0.07	0.47	0.04	-0.41	-0.69	-0.91	-1.14	-0.85	-0.90	-1.26	-1.11	-0.96	-0.75	-0.36	0.03	-0.40	-0.02	0.31	0.52
M	-1.13	0.69	0.76	0.72	0.45	-0.20	-0.44	-0.54	-0.78	-0.90	-1.20	-1.27	-1.07	-1.07	-0.92	-0.91	-0.74	-0.16	0.06	0.07	-0.03	-1.86
	1.08	0.86	0.53	0.17	0.50	0.08	-0.30	-0.63	-0.88	-1.14	-0.91	-0.95	-1.27	-1.08	-0.90	-0.64	-0.32	0.06	-0.30	0.03	0.33	0.53
N	-0.74	0.90	0.90	0.80	0.45	-0.20	-0.40	-0.48	-0.71	-0.84	-1.21	-1.27	-1.01	-0.99	-0.85	-0.86	-0.73	-0.14	0.15	0.22	0.19	-1.47
	1.08	0.83	0.54	0.25	0.54	0.10	-0.20	-0.54	-0.76	-0.98	-0.83	-0.87	-1.11	-0.96	-0.81	-0.54	-0.28	0.10	-0.21	0.05	0.31	0.54
O	-1.01	0.98	1.09	1.03	0.94	0.26	-0.29	-0.42	-0.58	-0.61	-0.63	-0.69	-0.78	-0.85	-0.78	-0.74	-0.26	0.36	0.40	0.42	0.28	-1.71
	0.21	0.60	0.51	0.31	0.54	0.11	-0.12	-0.47	-0.56	-0.70	-0.71	-0.75	-0.82	-0.76	-0.73	-0.44	-0.26	0.12	-0.14	0.02	0.10	-0.31
P		0.00	1.11	0.97	0.59	0.27	-0.01	-0.06	-0.40	-0.49	-0.54	-0.59	-0.65	-0.66	-0.40	-0.43	-0.22	0.03	0.36	0.46	-0.67	
		-0.23	0.48	0.27	0.68	0.29	-0.12	-0.40	-0.29	-0.41	-0.53	-0.57	-0.53	-0.47	-0.65	-0.43	-0.07	0.27	-0.17	0.01	-0.72	
Q		-1.39	0.96	1.09	0.77	0.38	-0.01	-0.08	-0.37	-0.43	-0.52	-0.57	-0.58	-0.61	-0.41	-0.41	-0.09	0.24	0.51	0.34	-2.02	
		-0.89	0.30	0.26	0.82	0.43	0.00	-0.21	-0.01	-0.18	-0.32	-0.36	-0.28	-0.18	-0.44	-0.29	0.09	0.43	-0.16	-0.15	-1.36	
R			-0.02	1.24	0.99	0.56	0.53	0.39	-0.31	-0.41	-0.51	-0.56	-0.55	-0.54	0.09	0.15	0.12	0.49	0.69	-0.60		
			-0.44	0.33	0.96	0.56	0.20	0.09	0.27	0.08	0.18	0.15	-0.02	0.11	-0.13	-0.07	0.24	0.60	-0.07	-0.87		
S			-0.89	1.37	1.23	0.81	1.12	1.17	1.16	1.14	0.85	0.81	1.01	0.95	0.88	0.77	0.40	0.76	0.85	-1.44		
			-0.74	0.37	1.10	0.76	0.40	0.42	0.46	0.25	0.68	0.65	0.16	0.31	0.22	0.15	0.47	0.76	0.00	-1.14		
T				0.07	1.87	1.72	1.45	1.32	1.23	1.16	0.88	0.84	1.04	1.03	1.05	1.12	1.33	1.42	-0.41			
				-0.65	0.95	0.96	0.72	0.71	0.69	0.48	0.96	0.93	0.39	0.54	0.52	0.49	0.68	0.64	-1.00			
U					-0.02	1.61	1.53	1.43	1.38	1.22	0.79	0.75	1.10	1.20	1.19	1.23	1.24	-0.42				
					-0.29	0.99	0.97	0.89	0.85	0.74	1.24	1.21	0.66	0.72	0.72	0.75	0.73	-0.59				
V						-0.72	-0.12	0.32	1.39	1.43	1.32	1.29	1.33	1.22	0.10	-0.40	-1.05					
						-0.15	0.34	0.12	0.88	1.12	1.44	1.41	1.04	0.76	-0.05	0.13	-0.39					
W									-0.55	-0.22	-0.62	-0.66	-0.31	-0.70								
									0.45	1.43	**1.61**	1.58	1.36	0.34								

Percent errors for CMFD (26 x 26 x12)

Percent errors for ANM (26 x 26 x 12)

Reference is the result of CMFD (104 x 104 x 48)

The maximum percent errors are shown in bold character

Figure 6: Comparison of Percent Errors of Channel Power Densities from CMFD (26 x 26 x 12) and ANM (26 x 26 x 12) for the Typical CANDU-6 Without Xenon Effect Problem

	1	2	3	4	5	6	7	8	9	10	11	12	13	14	15	16	17	18	19	20	21	22
A									0.89	0.97	1.02	1.02	0.97	0.89								
									0.89	0.98	1.02	1.02	0.98	0.89								
B						0.78	0.96	1.12	1.24	1.33	1.37	1.37	1.33	1.24	1.12	0.96	0.78					
						0.79	0.96	1.12	1.24	1.33	1.37	1.37	1.33	1.24	1.12	0.96	0.79					
C					0.89	1.11	1.30	1.45	1.56	1.63	1.66	1.66	1.63	1.56	1.45	1.30	1.11	0.89				
					0.89	1.11	1.30	1.45	1.55	1.63	1.66	1.66	1.63	1.55	1.45	1.30	1.11	0.89				
D				0.91	1.17	1.40	1.57	1.68	1.76	1.81	1.83	1.83	1.81	1.76	1.69	1.57	1.40	1.17	0.91			
				0.91	1.17	1.40	1.56	1.68	1.75	1.80	1.82	1.82	1.80	1.75	1.68	1.56	1.40	1.17	0.91			
E			0.85	1.15	1.42	1.61	1.73	1.79	1.81	1.83	1.84	**1.84**	1.83	1.81	1.79	1.73	1.61	1.42	1.15	0.86		
			0.86	1.15	1.41	1.61	1.72	1.78	1.80	1.82	1.83	**1.83**	1.82	1.80	1.78	1.72	1.61	1.41	1.15	0.86		
F			1.06	1.37	1.60	1.74	1.78	1.77	1.70	1.69	1.71	1.71	1.69	1.70	1.77	1.79	1.74	1.61	1.37	1.07		
			1.07	1.37	1.60	1.73	1.78	1.76	1.70	1.68	1.70	1.70	1.68	1.70	1.76	1.78	1.73	1.60	1.37	1.07		
G		0.91	1.25	1.54	1.73	1.80	1.75	1.69	1.61	1.58	1.59	1.59	1.58	1.61	1.69	1.76	1.81	1.73	1.54	1.25	0.92	
		0.92	1.25	1.53	1.72	1.79	1.75	1.68	1.60	1.57	1.59	1.59	1.57	1.60	1.68	1.75	1.79	1.72	1.53	1.25	0.92	
H		1.07	1.40	1.65	1.79	1.81	1.71	1.62	1.53	1.49	1.50	1.50	1.49	1.53	1.62	1.71	1.82	1.80	1.66	1.41	1.08	
		1.07	1.40	1.65	1.78	1.80	1.70	1.61	1.52	1.49	1.50	1.50	1.49	1.52	1.61	1.70	1.80	1.78	1.65	1.40	1.07	
J	0.86	1.21	1.52	1.72	1.81	1.75	1.64	1.53	1.46	1.43	1.43	1.43	1.43	1.46	1.54	1.64	1.76	1.81	1.73	1.52	1.21	0.86
	0.86	1.20	1.51	1.71	1.80	1.74	1.63	1.53	1.45	1.42	1.43	1.43	1.42	1.45	1.53	1.63	1.74	1.80	1.71	1.51	1.20	0.86
K	0.95	1.30	1.59	1.76	1.79	1.70	1.58	1.48	1.41	1.38	1.39	1.39	1.38	1.41	1.48	1.58	1.70	1.79	1.76	1.59	1.30	0.95
	0.95	1.29	1.58	1.74	1.77	1.68	1.57	1.47	1.40	1.37	1.38	1.38	1.37	1.40	1.47	1.57	1.68	1.77	1.75	1.58	1.29	0.95
L	1.00	1.34	1.62	1.77	1.77	1.67	1.55	1.45	1.38	1.36	1.36	1.36	1.36	1.39	1.45	1.55	1.67	1.78	1.78	1.63	1.35	1.00
	1.00	1.34	1.61	1.76	1.76	1.65	1.54	1.44	1.38	1.35	1.35	1.35	1.35	1.38	1.44	1.54	1.65	1.76	1.76	1.61	1.34	1.00
M	1.00	1.34	1.62	1.77	1.77	1.67	1.55	1.45	1.38	1.35	1.36	1.36	1.35	1.38	1.45	1.55	1.67	1.77	1.77	1.63	1.35	1.00
	0.99	1.33	1.61	1.75	1.75	1.65	1.53	1.44	1.37	1.34	1.35	1.35	1.34	1.37	1.44	1.53	1.65	1.75	1.75	1.61	1.33	0.99
N	0.95	1.29	1.58	1.75	1.78	1.69	1.57	1.47	1.40	1.37	1.38	1.38	1.37	1.40	1.47	1.57	1.69	1.78	1.76	1.59	1.30	0.95
	0.94	1.29	1.57	1.73	1.76	1.67	1.55	1.46	1.39	1.36	1.36	1.36	1.36	1.39	1.46	1.56	1.67	1.76	1.73	1.57	1.29	0.94
O	0.85	1.20	1.50	1.71	1.79	1.73	1.62	1.52	1.44	1.41	1.42	1.42	1.41	1.44	1.52	1.62	1.74	1.80	1.71	1.51	1.20	0.86
	0.85	1.19	1.49	1.69	1.77	1.71	1.60	1.50	1.43	1.40	1.40	1.40	1.40	1.43	1.50	1.60	1.71	1.77	1.69	1.49	1.19	0.85
P		1.06	1.38	1.63	1.76	1.78	1.68	1.59	1.50	1.47	1.48	1.48	1.47	1.50	1.59	1.68	1.78	1.77	1.63	1.38	1.06	
		1.05	1.37	1.61	1.74	1.76	1.66	1.57	1.48	1.45	1.46	1.46	1.45	1.48	1.57	1.66	1.76	1.74	1.61	1.37	1.05	
Q		0.89	1.22	1.50	1.68	1.76	1.71	1.65	1.57	1.54	1.56	1.56	1.54	1.57	1.65	1.71	1.76	1.69	1.50	1.22	0.90	
		0.89	1.21	1.48	1.66	1.73	1.69	1.63	1.55	1.52	1.54	1.54	1.52	1.55	1.63	1.69	1.73	1.66	1.48	1.21	0.89	
R			1.03	1.32	1.55	1.68	1.73	1.72	1.66	1.65	1.67	1.67	1.65	1.66	1.72	1.73	1.69	1.55	1.32	1.03		
			1.02	1.31	1.53	1.66	1.70	1.69	1.63	1.62	1.64	1.64	1.62	1.63	1.69	1.70	1.66	1.53	1.31	1.02		
S			0.82	1.10	1.36	1.55	1.67	1.73	1.76	1.78	1.79	1.79	1.78	1.76	1.73	1.67	1.55	1.36	1.11	0.82		
			0.82	1.10	1.35	1.53	1.64	1.71	1.73	1.75	1.76	1.76	1.75	1.73	1.71	1.64	1.53	1.35	1.10	0.82		
T				0.87	1.12	1.34	1.51	1.63	1.70	1.75	1.78	1.78	1.75	1.71	1.63	1.51	1.34	1.12	0.87			
				0.86	1.11	1.32	1.49	1.60	1.68	1.72	1.75	1.75	1.73	1.68	1.60	1.49	1.32	1.11	0.86			
U					0.85	1.06	1.25	1.40	1.51	1.58	1.61	1.62	1.58	1.51	1.40	1.25	1.06	0.85				
					0.84	1.05	1.23	1.38	1.49	1.56	1.59	1.59	1.56	1.49	1.38	1.24	1.05	0.84				
V						0.75	0.92	1.08	1.20	1.29	1.33	1.33	1.29	1.20	1.08	0.93	0.75					
						0.75	0.92	1.07	1.19	1.27	1.31	1.31	1.27	1.19	1.07	0.92	0.75					
W									0.86	0.94	0.99	0.99	0.94	0.86	----------*without xenon effect*							
									0.85	0.93	0.98	0.98	0.93	0.85	----------*with xenon effect*							

Reference is the result of CMFD (104 x 104 x 48)

The maximum normalized bundle power densities are shown in bold character

Figure 7: Xenon effect on normalized bundle power densities at plane 6 of typical CANDU-6 problem for ANM (26 x 26 x 12)

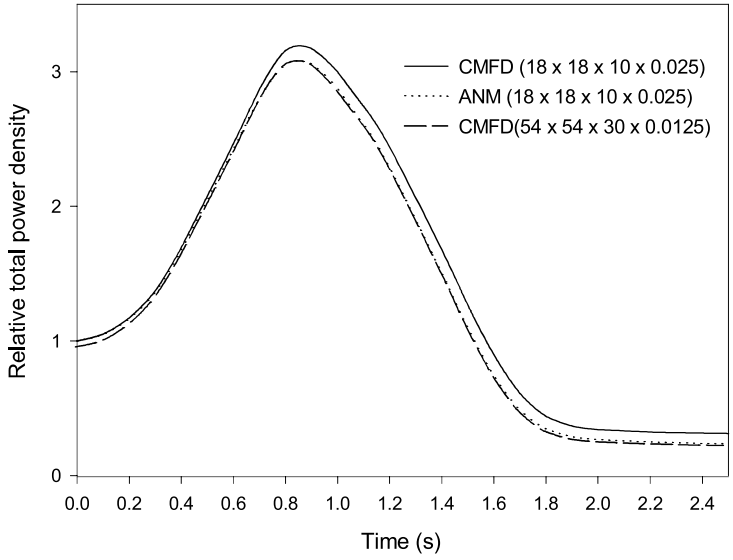

Figure 8: Relative total power density versus time for the CANDU benchmark problem (time step =0.025s)

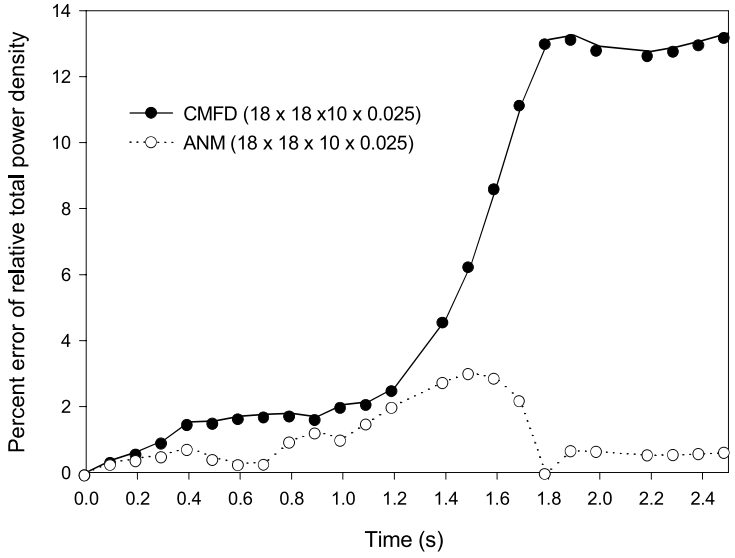

Figure 9: Percent error of relative total power density versus time for the CANDU benchmark problem (time step = 0.025s)

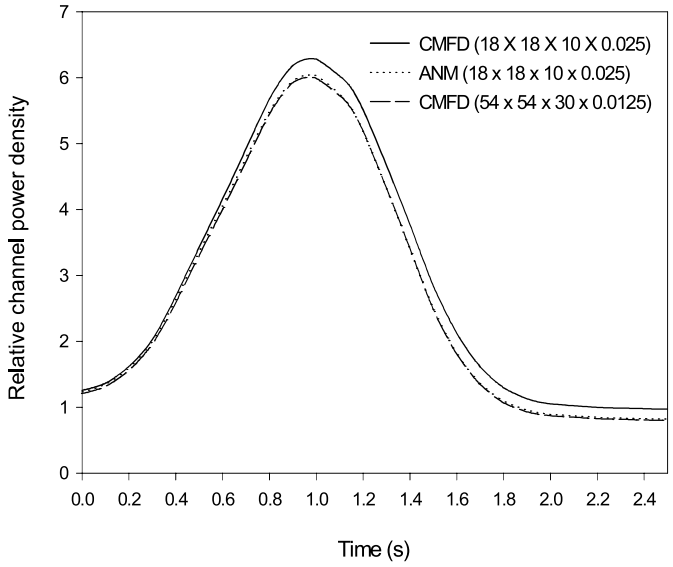

Figure 10: Relative channel power density of channel (5,10) versus time for the CANDU benchmark problem (time step = 0.025s)

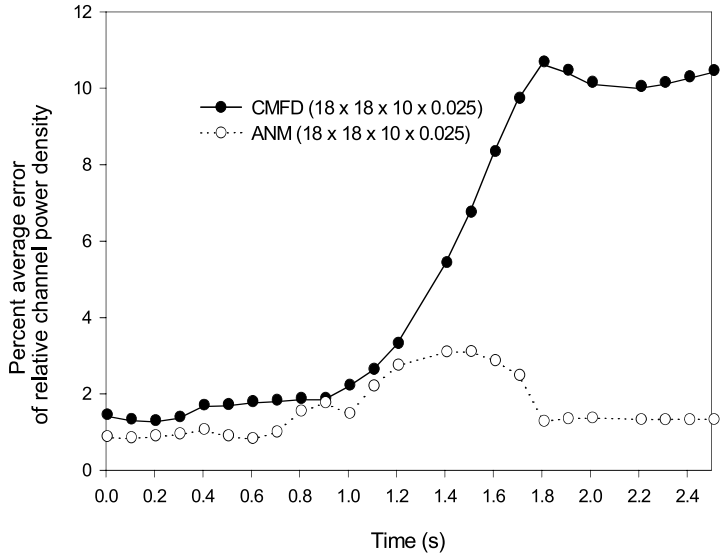

Figure 11: Percent average error of relative channel power density versus time for the CANDU benchmark problem (time step =0.025s)

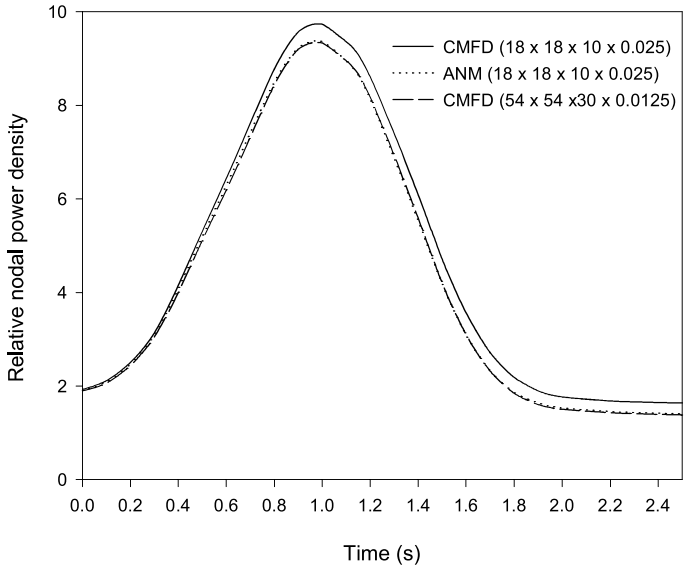

Figure 12: Relative nodal power density of bundle (6,10,5) versus time for the CANDU benchmark problem (time step = 0.025s)

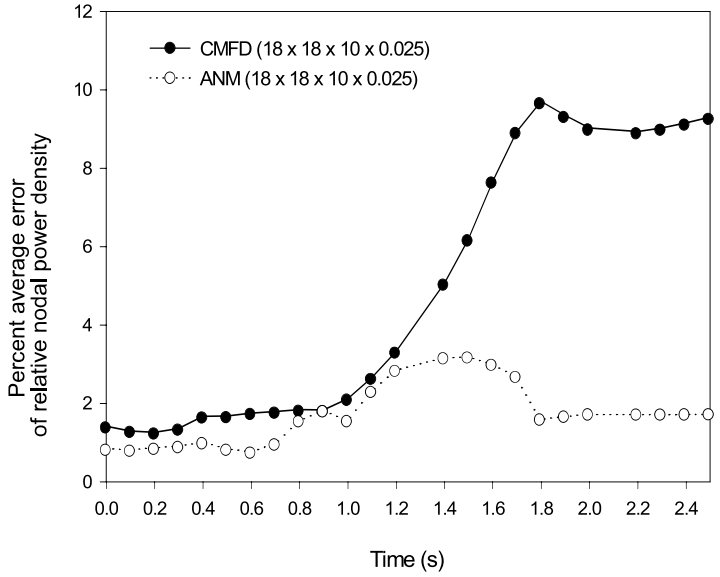

Figure 13: Percent average error of relative nodal power density versus time for the CANDU benchmark problem (time step = 0.025s)

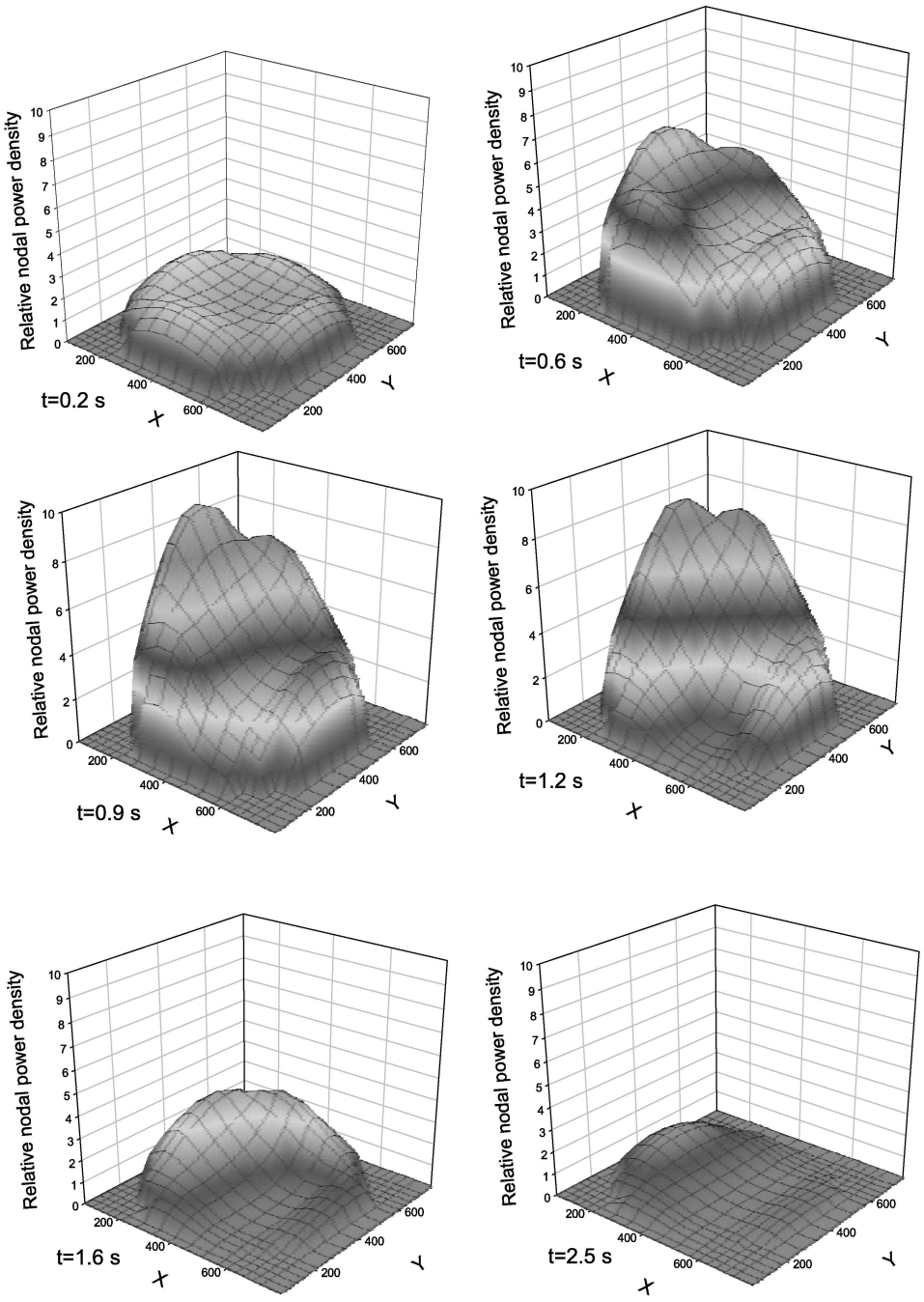

Figure 14: Relative nodal power density distributions versus time on plane 5 of the CANDU benchmark problem for ANM (time step = 0.025s)

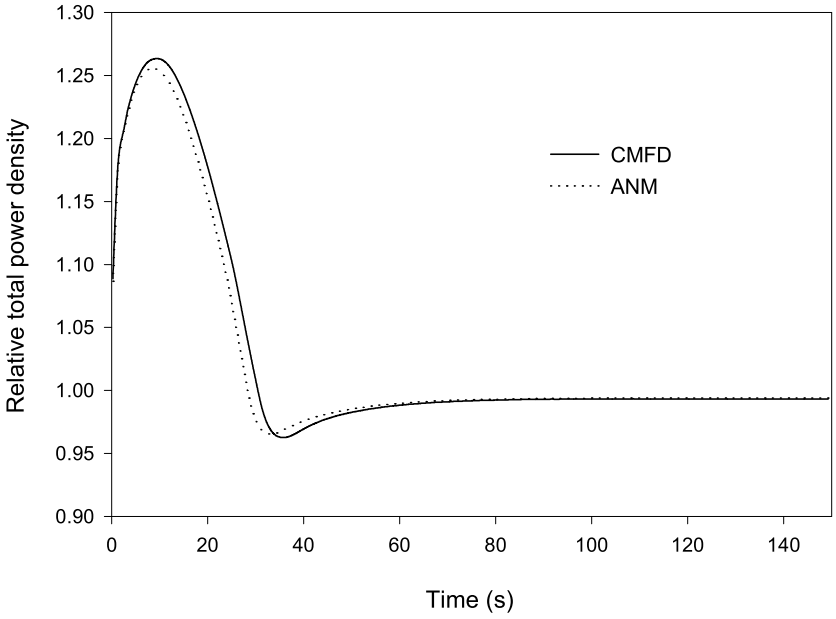

Figure 15: Relative total power density versus time for the typical CANDU-6 problem

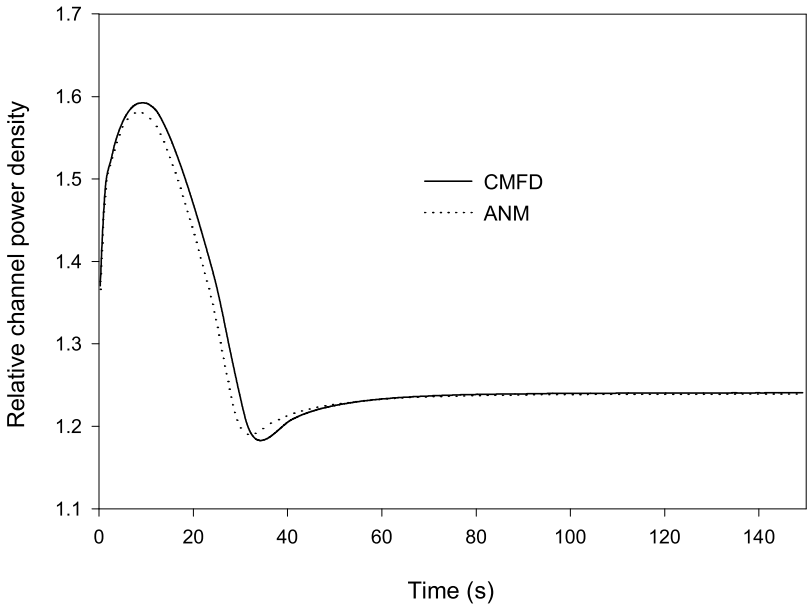

Figure 16: Relative channel power density of channel (E12) versus time for the typical CANDU-6 problem

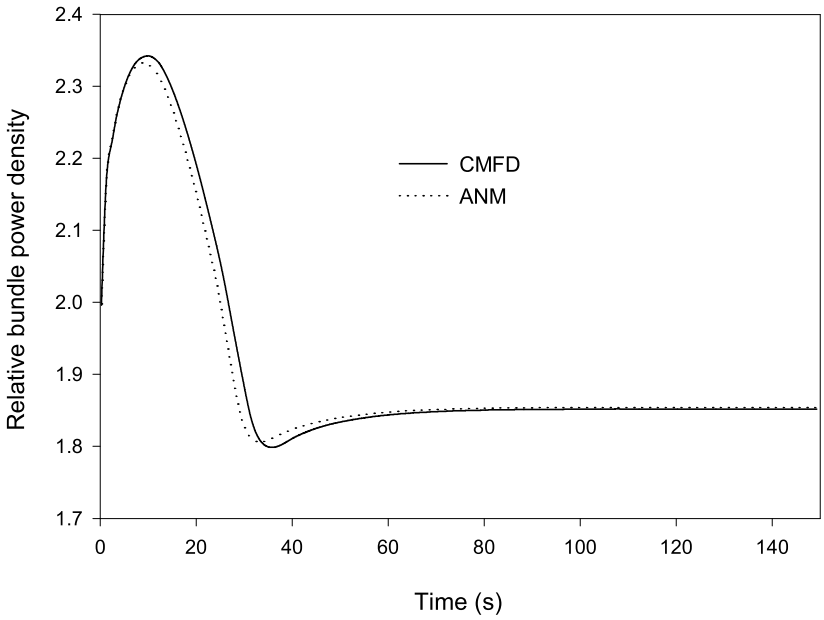

Figure 17: Relative bundle power density of bundle (E12,6) versus time for the typical CANDU-6 problem

8. REFERENCES

ANL, (1985). National Energy Software Center: Benchmark Problem Book. ANL-7416, pp.699-710, Argonne National Laboratory, United States.

FINNEMANN, F. BENNEWITZ, and WAGNER, M. R. (1977). Interface Current Techniques for Multi-dimensional Reactor Calculations. Atomkernenergie, Vol. 30, No.1, pp. 123.

HENRY, A. F. (1975). Nuclear Reactor Analysis. M.I.T. Press, Cambridge, Massachusetts.

KAVEH, S., KOCLAS, J. and ROY R. (1999). Simulation of CANDU Reactor Transients Using Hierarchical Supernodal Analysis, CNS Proceedings, Montreal, Canada.

KOCLAS, J. (1998). Comparisons of the Different Approximations Leading to Mesh Centered Finite Differences Starting from the Analytic Nodal Method. Annals of Nuclear Energy, Vol. 25, No.11, pp. 821-838.

LAWRENCE, R. D. and DORNING, J. J. (1980). A Nodal Green's Function Method for Multi-dimensional Neutron Diffusion Calculations. Nuclear Science and Engineer, Vol. 76, pp. 218.

MAO, J. (2000). Implementation of the Analytic Nodal Method in the Code NDF and Applications to the CANDU Reactors. MScA Thesis, Institut de Génie Nucléaire, École Polytechnique de Montréal, Université de Montréal (to be published).

MARLEAU, G., HEBERT, A. and ROY, R. (1993). New Computational Methods Used in the Lattice Code DRAGON. Topical Meeting on Advances in Reactor Physics, Charleston, SC, 8-11.

MARLEAU, G., ROY, R. and ARESENAULT, B. (1994). Simulation of Reactivity Control Devices in a CANDU-6 Reactor using DRAGON. CNS Proceedings, Pembroke, Ontario, Canada.

MARLEAU, G., HÉBERT, A. and ROY, R. (1996). A User's Guide for DRAGON. Report IGE-174 Rev 1, École Polytechnique de Montréal, Canada.

NAVARRO ARIAS, S. H. (1996). Étude Numérique des Effets de Diffusion Directionnels dan le Cœur du Réacteur GENTILLY-2. MSc. Thesis, Université de Montréal

ROY, R., MARLEAU, G., TAJMOUATI, J. and ROZON, D. (1993). Modeling of CANDU Reactivity Control Devices with the Lattice Code DRAGON. Annals of Nuclear Energy, Vol. 21, No.2, pp. 115-132.

SMITH, K. S. (1979). An Analytical Nodal Method for Solving the Two-group, Multi-dimensional, Static and Transient Neutron Diffusion Equations. MSc. Thesis, Massachusetts Institute of Technology.

Appendix A The 3-D CANDU Benchmark Problem

Geometry

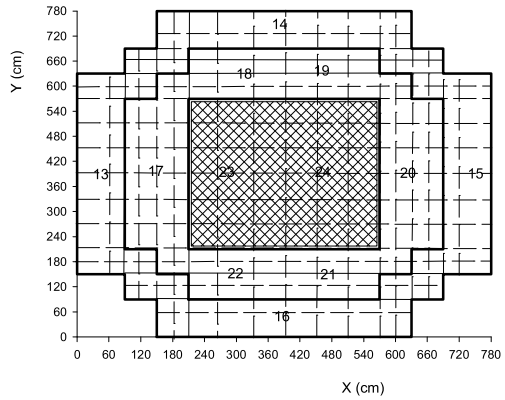

Figure A1.1: Initial back view of reactor for the CANDU benchmark problem

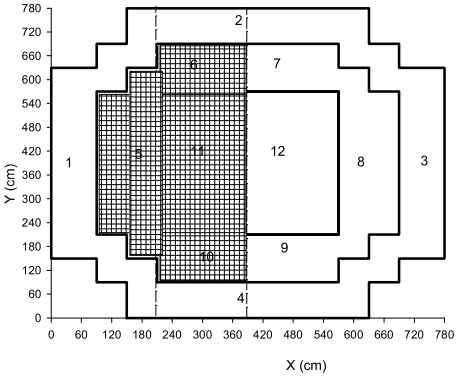

Figure A1.2: Reactor region affected by voiding for the CANDU benchmark problem

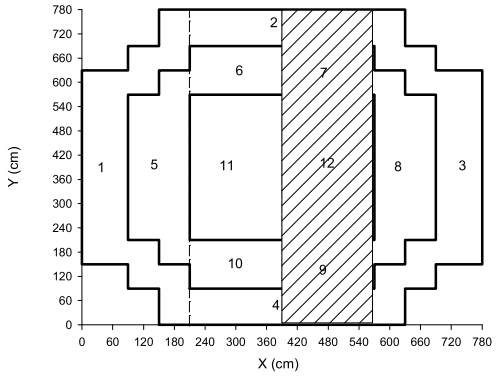

Figure A1.3: Reactor region affected by the system in front half of the reactor for the CANDU benchmark problem

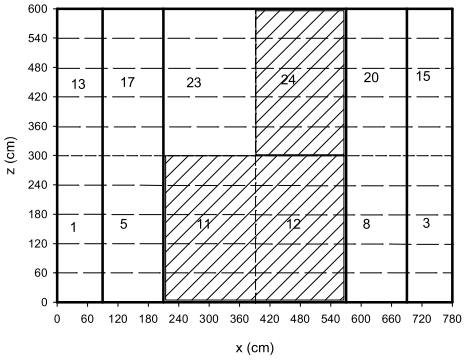

Figure A1.4: Reactor region affected by the shutdown shutdown system in horizontal cross-section at Y=390cm for the CANDU benchmark problem

The Material Properties are given in (ANL, 1985).

Appendix B The Typical CANDU-6 Problem

Geometry

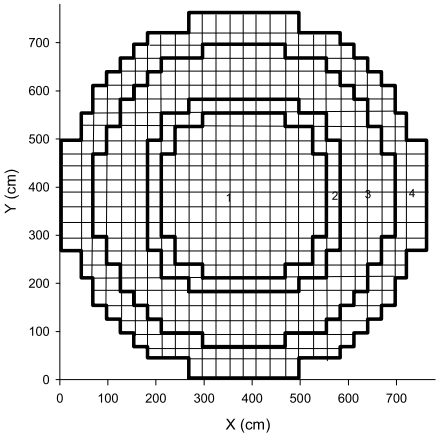

Figure A1.5: Vertical cross-section at Z=0 cm illustrating grid layout in XY plane of the typical CANDU-6 problem

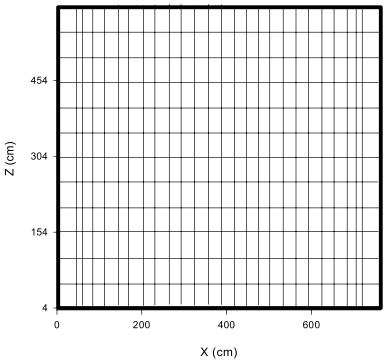

Figure A1.6: Horizontal cross-section at Y=382.85cm illustrating grid layout in the XZ plane of the typical CANDU-6 problem

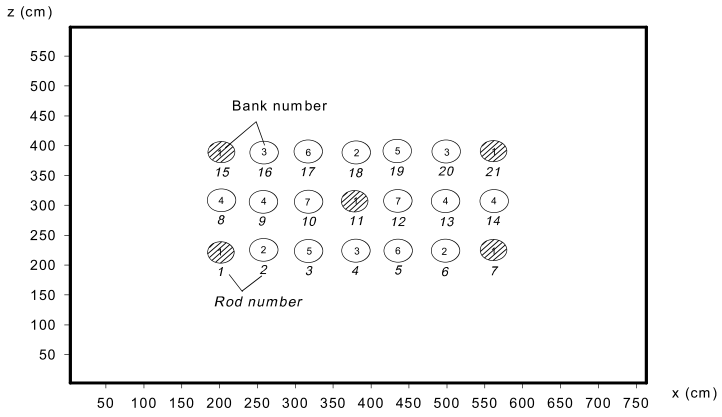

The instantaneous withdrawal rods: No.1, No 7, No.11, No. 15 and No. 21
Figure A1.7: Adjust location in the typical CANDU-6 problem

The Material Properties are given in (Mao, 2000)

Perturbation:

A group of rods are ejected from the reactor core at beginning. Figure A1.7 shows the location of these rods. The response of the reactor regulation system and the incremental cross-section are calculated by DRAGON/DONJON chain code.